Finite aperture Fraunhofer holograms of two co-planar discs

P.R. Hobson and A. Raouf

Laser Applications Group, Department of Physics, Brunel University
Uxbridge, Middlesex, UB8 3PH, UK

ABSTRACT

In this paper we present a theoretical model describing the real images replayed from finite aperture Fraunhofer holograms of two identical co-planar objects. We have solved numerically the resulting image equations for the case of two circular disc objects, and compare our predictions with experimental measurements from in-line Fraunhofer holograms recorded on silver-halide emulsions. Three measurement criteria for calculating the disc diameters and separation are described, and their errors discussed. It is found experimentally that a criterion based on average intensity results in the smallest errors due to its insensitivity to the effects of coherent noise.

1. INTRODUCTION

In-line Fraunhofer holography is an important technique for simultaneously recording large volumes of small particulates at high resolution[1]. From the reconstructed images both particle size and three-dimensional position information can be determined. In many applications a detailed understanding of the errors arrising from such measurements is essential[2-4].

There is considerable interest in extending the theory to the case of two co-planar discs for the following reasons: firstly in many cases e.g. bubble chamber vapour bubbles showing the tracks of ionizing particles, or droplets in a fuel spray, one often finds touching or near-touching particles approximately located in a common depth plane. In these two examples the disc diameters will be locally uniform. Secondly results from the two object case should be valid for most multi-object in-line holograms because of the sparse density of the objects over the total hologram field; a requirement for making good in-line holograms is that less than 1% of the object beam is obscured.

Belz and Shofner[5] studied in detail the intensity distribution in the region of the real image for the case of a single opaque disc and a finite hologram aperture. Such an aperture will arrise from the finite size of the hologram, the film MTF, and noise in the recording and reconstruction processes.

In this paper we present an extension of this work to the case of two distinct co-planar objects, and calculate the intensity distribution in the vicinity of the real image for an aperture-limited Fraunhofer hologram.

The intensity distributions in the real image for various limiting apertures were calculated and are compared with reconstructed images from a Fraunhofer hologram of a precision test object. Three different criteria for determining disc diameter and separation are described and their errors discussed. From measurements made at different defocus positions an algorithm for determining the true focal plane is proposed. All aspects of this paper are discussed in greater detail by Raouf[6].

2. THEORETICAL

The reconstructed image field from a finite aperture hologram for a single opaque disc has previously been calculated[5]. In this paper we derive an equation for the three-dimensional image intensity for an object consisting of two coplanar opaque discs. This equation is solved numerically and the results are experimentally verified in section 3. For mathematical simplicity we have considered only the special (but important) case of collimated recording and replay beams. Figure 1 shows the coordinate systems of the object, hologram, and image planes.

2.1 Diffracted field recorded on hologram

The far-field diffraction pattern, at a distance Z_1, for a two-dimensional object distribution $A(\varepsilon,\eta)$ when illuminated by an infinite plane wave of wavelength λ and amplitude B, is given by (Tyler and Thompson[7]):

$$I(x,y) = B^2 \left\{ \begin{array}{c} 1 + \dfrac{1}{\lambda^2 Z_1^2} \widetilde{A}(\dfrac{x}{\lambda Z_1},\dfrac{y}{\lambda Z_1})\ \widetilde{A}^*(\dfrac{x}{\lambda Z_1},\dfrac{y}{\lambda Z_1}) \\ \\ -\dfrac{2}{\lambda Z_1}\left[\sin(\dfrac{\pi r^2}{\lambda Z_1})\mathrm{Re}\ \widetilde{A}(\dfrac{x}{\lambda Z_1},\dfrac{y}{\lambda Z_1})+\cos(\dfrac{\pi r^2}{\lambda Z_1})\mathrm{Im}\ \widetilde{A}(\dfrac{x}{\lambda Z_1},\dfrac{y}{\lambda Z_1}) \right] \end{array} \right\} \qquad (1)$$

where $r^2 = x^2 + y^2$,

$$\frac{\pi\ (\varepsilon^2 + \eta^2)}{\lambda\ Z_1} \ll 1$$

and

$$\widetilde{A}(\frac{x}{\lambda Z_1},\frac{y}{\lambda Z_1}) = \int_{-\infty}^{\infty}\int_{-\infty}^{\infty} A(\varepsilon,\eta)\ \exp\ \{-2\pi i\ [\varepsilon\ \frac{x}{\lambda Z_1} + \eta\ \frac{y}{\lambda Z_1}]\}d\varepsilon.d\eta$$

is the Fourier transform of the object distribution.

Consider an object consisting of two co-planar opaque discs each of radius a with centres separated by a distance $2b$ such that $b \geq a$. Applying the Fourier addition and shift theorems, the intensity given by equation (1) may be written as

$$I(x,y) = B^2 \left\{ \begin{array}{c} 1 + \dfrac{4}{(\lambda Z_1)^2}\left[\widetilde{A}(\dfrac{x}{\lambda Z_1},\dfrac{y}{\lambda Z_1}).\cos(2\pi bs) \right]^2 \\ \\ -\dfrac{4}{\lambda Z_1}\sin(\dfrac{\pi r^2}{\lambda Z_1})\left[\widetilde{A}(\dfrac{x}{\lambda Z_1},\dfrac{y}{\lambda Z_1}).\cos(2\pi bs) \right] \end{array} \right\} \qquad (2)$$
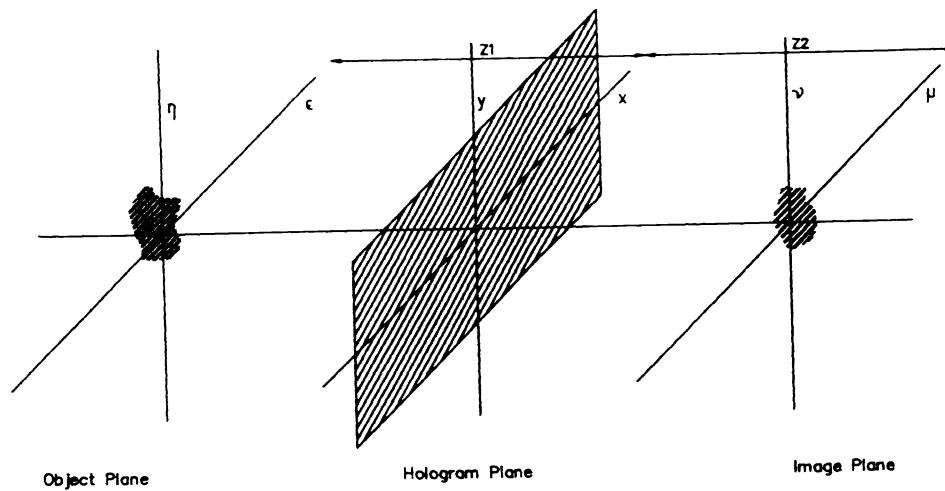
Figure 1. Coordinate systems used in the theoretical analysis.

where B and λ are the amplitude and wavelength of the illuminating wave.
The Fourier transform of a circular object of radius a is given by:

$$\tilde{A}\left(\frac{x}{\lambda Z_1}, \frac{y}{\lambda Z_1}\right) = (\pi a^2) \frac{2J_1(kar)\big/Z_1}{kar\big/Z_1}$$

where J_1 is the Bessel function of the first kind of order 1.

Hence the intensity recorded on a hologram at a distance Z_1 from the discs is given by

$$I(x,y) = B^2 \left\{ \begin{array}{l} 1 + 4\left(\frac{a}{r}\right)^2 \left[J_1\left(\frac{kar}{Z_1}\right)\right]^2 \left[\cos^2(\phi)\right] \\[3mm] -4\left(\frac{a}{r}\right)\sin\left(\frac{kr^2}{2Z_1}\right)\left[J_1\left(\frac{kar}{Z_1}\right). \cos(\phi)\right] \end{array} \right\} \tag{3}$$

where

$$k = \frac{2\pi}{\lambda}, \quad \text{and}\,\phi = 2\pi bs = \frac{kbx}{Z_1}$$

is the phase difference of the two diffracted waves arising from the two discs. A computer plot of equation (3) for typical recording parameters is shown in figure 2.
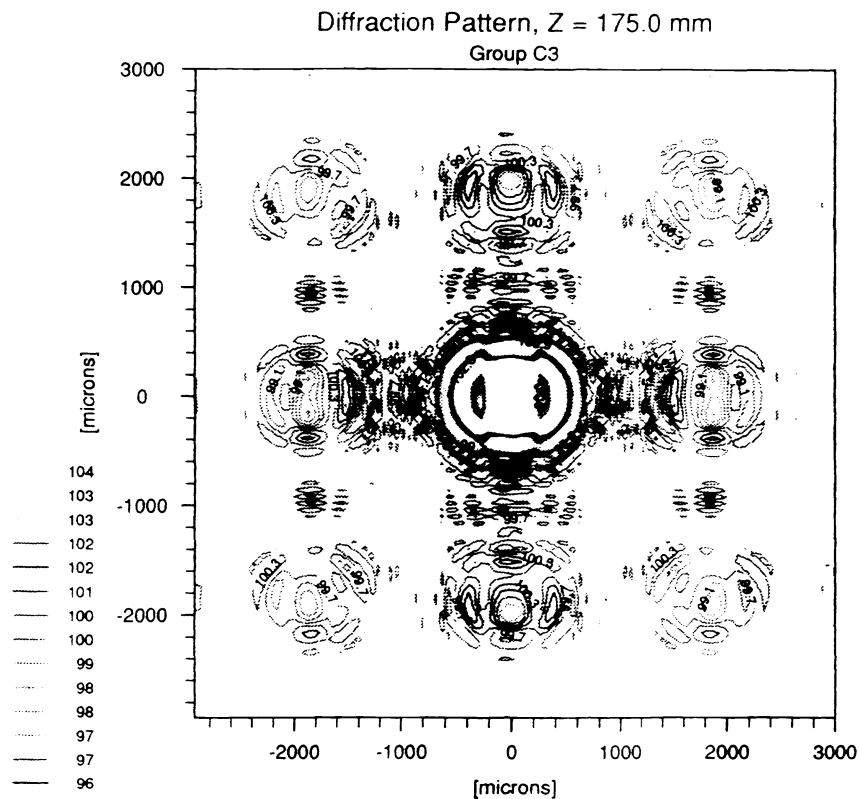
Diffraction Pattern, Z = 175.0 mm

Group C3

3000

2000

1000

[microns]

0

104
103
103
—— 102
—— 102
—— 101
—— 100 -1000
---- 100
.... 99
...... 98
.... 98
...... 97
—— 97
—— 96

-2000

-2000   -1000   0   1000   2000   3000

[microns]

Figure 2. Hologram plane diffraction pattern for two 150 μm diameter discs separated by $2b = 300$ μm.

2.2 Reconstructed image field

Making the usual simplifying assumptions of linear transmittance versus exposure at recording, and equal wavelengths in recording and reconstruction, the reconstructed field at a distance Z_2 from the hologram is given by

$$\psi(\mu,\nu) = -\frac{iC}{\lambda Z_2} \exp(ikZ_2)\int_{-\infty}^{\infty}\int_{-\infty}^{\infty} I(x,y)\ \exp\{\frac{ik}{2Z_2}\ [(\mu-x)^2+ (\nu-y)^2]\}dx.dy$$

where $I(x,y)$ is defined by equation (3), and C is the amplitude of the reconstructing beam. The third term in equation (3) represents the interference between the diffracted waves from the two discs and the coherent background and is responsible for producing the real and virtual images in the reconstruction.

Writing

$$I(x,y) = 4a\ B^2\ P(x,y)\ \sin(\theta_1)\cos(\phi\ )$$

where

$$P(x,y) = \frac{1}{\sqrt{x^2 + y^2}}\ J_1(\frac{ka\sqrt{x^2 + y^2}}{Z_1})$$

$$\theta_1 = \frac{k(x^2 + y^2)}{Z_1}$$

and defining

$$\theta_2 = \frac{k}{2Z_2}(x^2 + y^2 - 2x\mu - 2y\nu)$$

and

$$\theta_3 = k(Z_2 + \frac{\mu^2 + \nu^2}{2Z_2})$$

the reconstructed field at distance Z_2 from the hologram is given by

$$\psi(\mu,\nu) = -\frac{4iaB^2C}{\lambda Z_2} \exp(i\theta_3) \int_{-\infty}^{\infty}\int_{-\infty}^{\infty} P(x,y) \cos(\phi)\sin(\theta_1)\exp(i\theta_2)dx.dy$$

Since we are only interested in the real image, we can write $\sin(\theta_1)$ in complex form and take only the negative exponential term (Belz[8]).

The image intensity, given by $I(\mu,\upsilon) = \Psi(\mu,\upsilon)\Psi^*(\mu,\upsilon)$, is

$$I(\mu,\nu) = \left(\frac{2aB^2C}{\lambda Z_2}\right)^2 \left\{ \left[\int_{-\infty}^{\infty}\int_{-\infty}^{\infty} P(x,y)\cos(\phi)\cos(\theta_1 - \theta_2)]\,dx.dy\right]^2 + \left[\int_{-\infty}^{\infty}\int_{-\infty}^{\infty} P(x,y)\cos(\phi)\sin(\theta_1 - \theta_2)]\,dx.dy\right]^2 \right\} \tag{4}$$

Consider the realistic case of a hologram where a finite aperture truncates the spatial extent of the diffracted wave recorded on the film. This aperture will be due to the finite extent of the film (or of the recording and replay beams), its finite resolution, and noise such as that arising from film grains. Assuming that the film MTF is constant up to the cut-off frequency, then, normalising the coordinates
$x = \rho_1 H$ and $y = \rho_2 H$ with

$$|\rho_1| \leq 1, |\rho_2| \leq 1$$

and writing $P(x,y)$, $(\theta_1 - \theta_2)$, and ϕ in terms of the limiting aperture H, we arrive finally at the following result

$$I(\mu,\nu) = (\frac{2aB^2CH}{\lambda Z_2})^2 \left\{ [\int_{-1}^{+1}\int_{-1}^{+1} \frac{1}{\sqrt{\rho_1^2 + \rho_2^2}} J_1(\Omega\sqrt{\rho_1^2 + \rho_2^2})\cos(W\frac{b}{a}\rho_1)\cos[\frac{U}{2}(\rho_1^2 + r_2^2) + W(\mu r_1 + \nu r_2)]d\rho_1.d\rho_2]^2 \right.$$

$$\left. + [\int_{-1}^{+1}\int_{-1}^{+1} \frac{1}{\sqrt{\rho_1^2 + \rho_2^2}} J_1(\Omega\sqrt{\rho_1^2 + \rho_2^2})\cos(W\frac{b}{a}\rho_1)\sin[\frac{U}{2}(\rho_1^2 + \rho_2^2) + W(\mu r_1 + \nu r_2)]d\rho_1.d\rho_2]^2 \right\} \tag{5}$$

with the normalized variables $\Omega = \frac{kaH}{Z_1}$, $W = \frac{kH}{Z_2}$, and $U = kH^2(\frac{1}{Z_1} - \frac{1}{Z_2})$

3. NUMERICAL SIMULATIONS

Equation 5, which describes the image formed from a finite aperture hologram, can only be solved numerically. It requires that the two -dimensional integrals are solved over a square domain. The integrands are oscillatory and include trigonometric functions with large radian arguments. Both of these aspects lead to the use of double precision variables and a high order of Gaussian Quadrature integration.

Gaussian Quadrature was chosen as the integration technique because of its ability to solve accurately integrals involving high order polynomials (an n-point technique will exactly solve a polynomial integral of order (2n-1)), and because of its simple extension to two dimensions. It should be noted that it is not the most efficient integrator for n-dimensions[9], but in practice it is usually the method of choice. A 96-point formula was chosen, with the coefficients and weights taken from Abramowitz and Stegun[10], and coded to 6 significant figures.

The images have planes of mirror symmetry about the μ and v axes, but are not symmetrical about the image plane.

4. EXPERIMENTAL RESULTS

To verify the theory developed in section 2, in-line holograms were made from a set of opaque discs on a precision test object. The replayed images from the developed hologram were imaged onto a video camera connected to a digital oscilloscope. These line scan images were transferred via an IEEE-488 bus to a PC for data storage and analysis.

4.1 The optical system

Figure 3 shows the layout of the optical system for recording and replay of the holograms.

A spatially filtered 5 mW He-Ne laser (λ = 633 nm) was expanded to a beam diameter of 50 mm by the telescope L1, L2. The shutter was used to control the energy at the hologram plane. During recording the test object was placed at a distance of 175.0 mm from the holographic plate. During replay the hologram was replaced in its recording position, and the real image was magnified by lens L3 onto the faceplate of an Ultricon video camera tube. The Ultricon (RCA 4532/U) was selected because of its uniform dark current and high resolution.

4.2 The holograms

A test object, consisting of several sets of pairs of opaque discs on a BK7 substrate, was placed 175.0 mm away from the hologram plane. The BK7 optical flat was 12.5 mm thick, with a surface flatness of $\lambda/10$ on both sides, and a surface quality of Scratch-Dig 10-5 (TecOptics, Isle of Man). The discs were deposited in Nichrome onto one side of the substrate by Datasights Ltd. The discs were placed on a 5 by 5 grid, with each row having a uniform disc diameter, and with each column having the same ratio of separation to diameter. The disc diameters varied from 50 microns to 300 microns, and the separations varied from touching discs to a separation of 4 times the diameter.

In the work reported here we used discs of 150 microns diameter, with centre-to-centre separations of 150, 250, and 300 microns.

The amplitude holograms were recorded on Agfa 8E75 HD plates developed in "LAZA Holograms" developer[11] and fixed. An OD of between 1.5 and 2.0 was found to give the best images. Great care was taken to minimise the coherent noise in the recording and replay system.

4.3 The data aquisition

The composite video signal from the camera was taken to two channels of an HP 54501A digital oscilloscope. One channel was used to provide a stable TV trigger from the desired line, while the other channel was used to display the video signal of that line. Each video scan line was averaged 32 times to increase the signal-to-noise ratio, then the fixed background arising from the non-uniformities in the Ultricon tube was digitally subtracted. The corrected scan line was transferred via IEEE-488 to a PC for further analysis, and to provide data storage and hardcopy.

The resolution of the Ultricon was determined to be 20 microns at the centre, and the raster scan was linear to better than 1% in this region.

5. COMPARISON OF NUMERICAL AND EXPERIMENTAL RESULTS

Holograms were recorded at a fixed value of Z_1 (175 mm), with the hologram aperture limited only by the finite film dimensions. During replay precise, square masks were located at the hologram plane to limit the aperture. These masks ranged in size from 1.8 x 1.8 mm^2 for $\Omega = 3.832$ to 9.2 x 9.2 mm^2 for $\Omega = 19.616$.

5.1 General image features

Figures 4,5,6 show some typical line scans from replayed holograms, and the results of the corresponding numerical caluculations. In each case the data are normalized to unity for the in-focus data at the geometrical centres of the disc images for a given separation and value of Ω.

Figure 4 shows intensity contour plots calculated by numerically solving equation 5, for $\Omega = 3.832$, 7.016, and 19.616 for two touching discs. Figure 5 shows a comparison of the numerical and experimental data for these values for in-focus images. A line scan through the two disc centres is shown. Figure 6 shows a set of linescans for different values of defocus for two discs separated by $2b = 300$ μm.

It can be seen that there is good qualitative agreement in all cases, the only significant difference being the additional noise present in the hologram images. The major features of planes of mirror symmetry, the dependence of the number of oscillations of the image on the number of zeros of J_1, and the increasing gradient of the edge of the disc image with W are all verified. High frequency effects, most clearly seen in figure 4 for W = 19.616 in the numerical simulation, are not so well reproduced in the experimental data. This may be due to two effects. Firstly the higher the value of W the larger distance over which fringes must be recorded on the hologram. However, although the fringe frequency does not change the modulation does decrease. Thus the features of the image which are encoded by the modulating envelope will be more susceptible to the effects of hologram noise for larger values of W. In addition the MTF of the combination of lens L3 and the video camera Ultricon tube will affect these rapidly varying parts of the image.

5.2 Size measurements

We adopted the three measurement criteria of Belz and Shofner[5], illustrated in figure 7, using them for both disc diameter and disc edge separation in the image plane.

W_{25} is the width measured at 25% of the intensity in the centre of the disc image, W_{50} is the width measured at 50% of the average disc intensity, and W_{edg} is the separation of the two outermost peaks in each disc image. The separation of the edges on a line joining the disc centres can also be calculated in an obvious way using these criteria.

Tables 1,2,3 present the measured diameters and separations using the three criteria W_{25}, W_{50}, and W_{edg} for both simulated and experimental images for values of Ω from 7.016 to 19.616.

Several trends are clear from the tables. For both simulated and experimental images the errors reduce for all three criteria as the value of Ω (which is related to the hologram resolution) increases. For simulated images the best criterion is W_{25}, whereas for experimental images W_{50} and W_{25} have similar errors. This is due to the insensitivity of W_{50} to noise in the replayed hologram image; the effects of noise were not modelled for the simulated images. The criterion W_{edg} always underestimates the disc diameter and thus overestimates the disc separation.
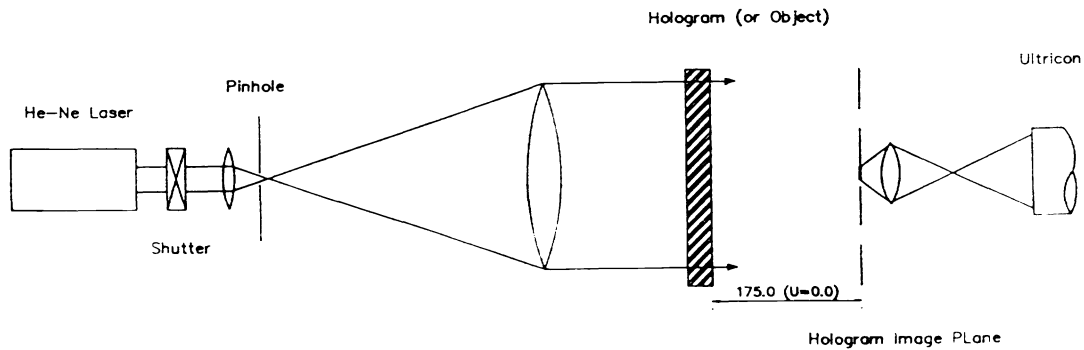
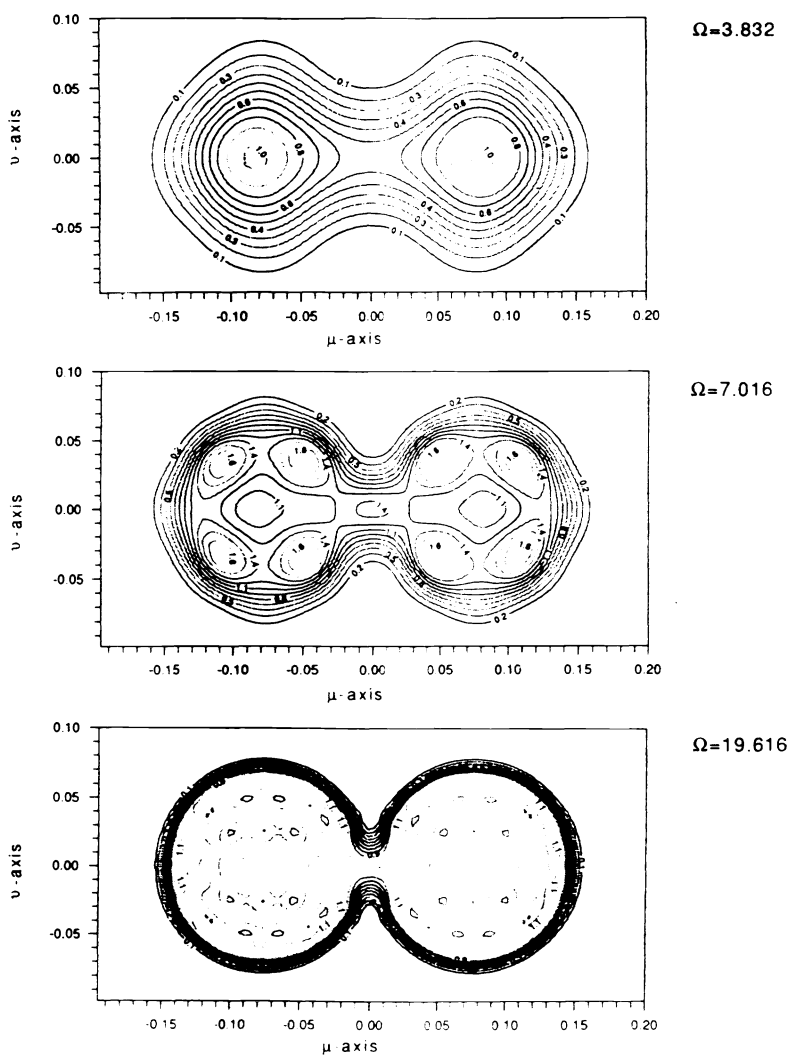Figure 3. Schematic of the optical system used in recording and replay.
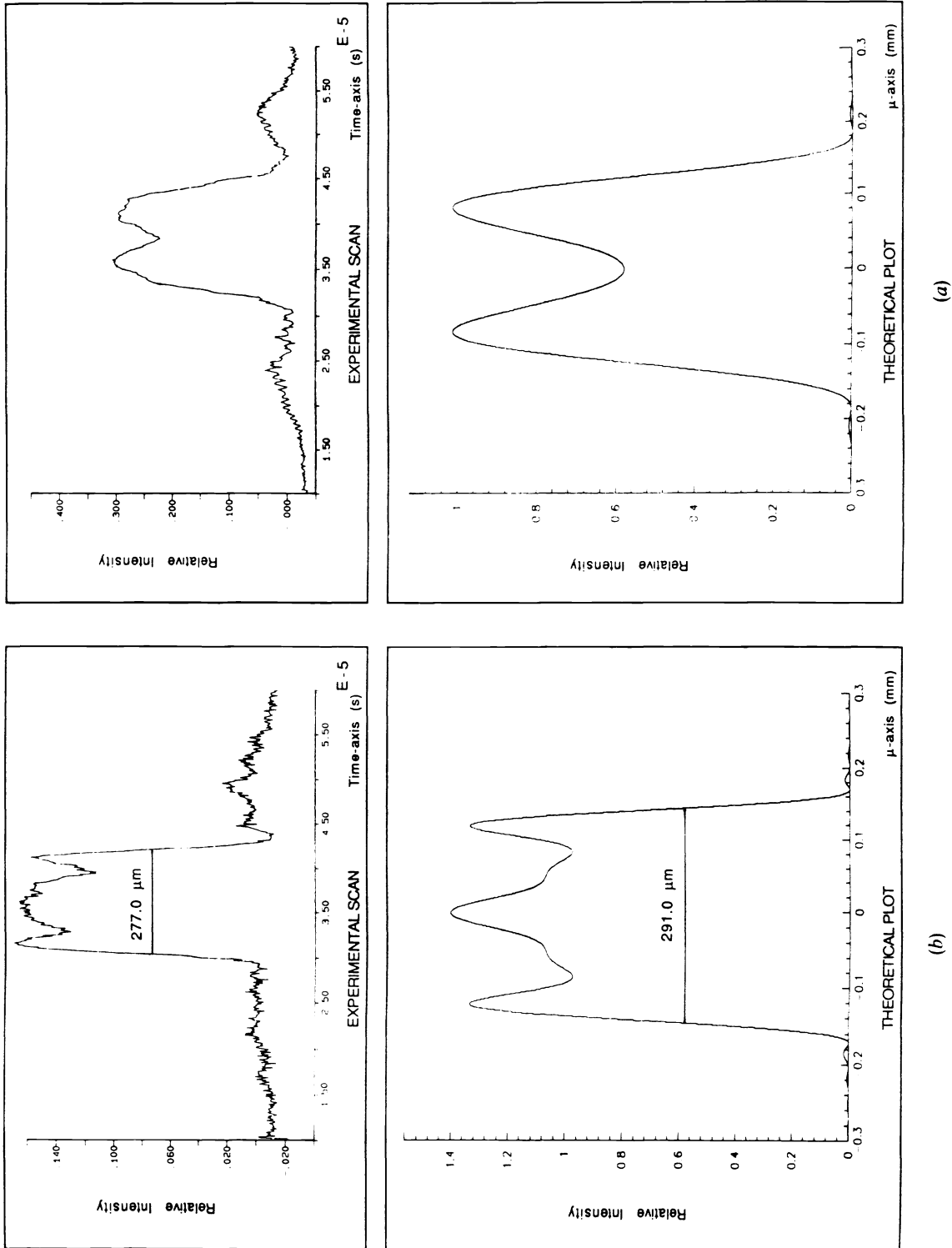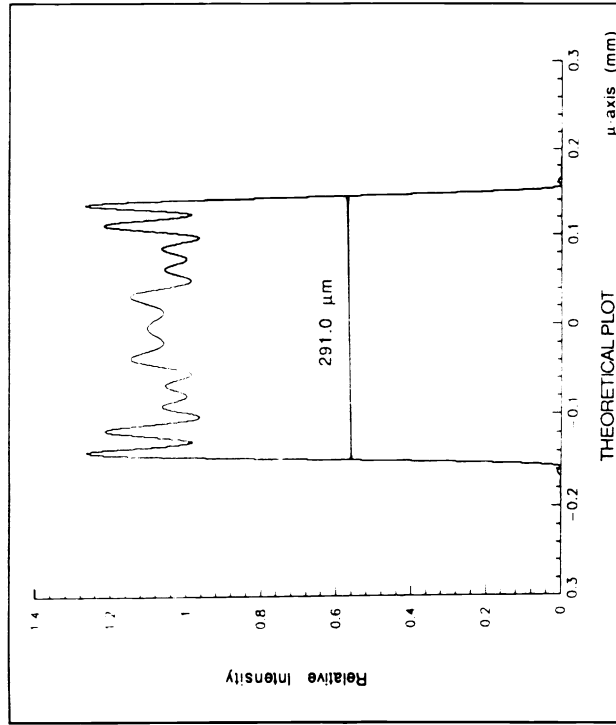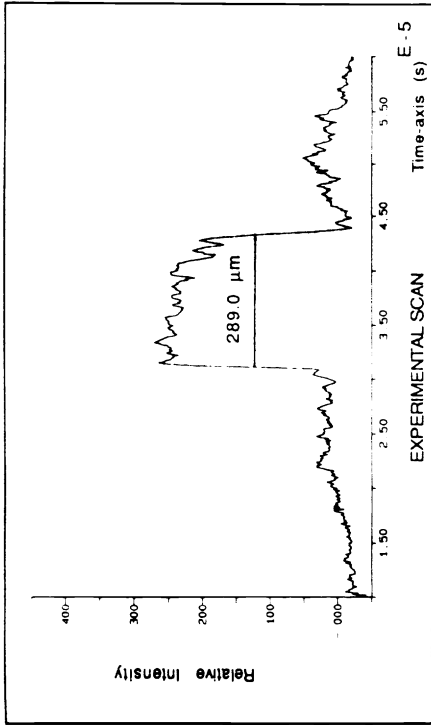

Figure 4. Numerically calculated focal-plane images of two touching discs for $\Omega = 3.832$, $\Omega = 7.016$, and $\Omega = 19.616$.

Figure 5. A comparison of experimental and numerically calculated focal-plane images for $\Omega = 3\cdot832$, $\Omega = 7\cdot016$, and $\Omega = 19\cdot616$. The figures show the intensity along a line joining the common centres of the two touching discs.
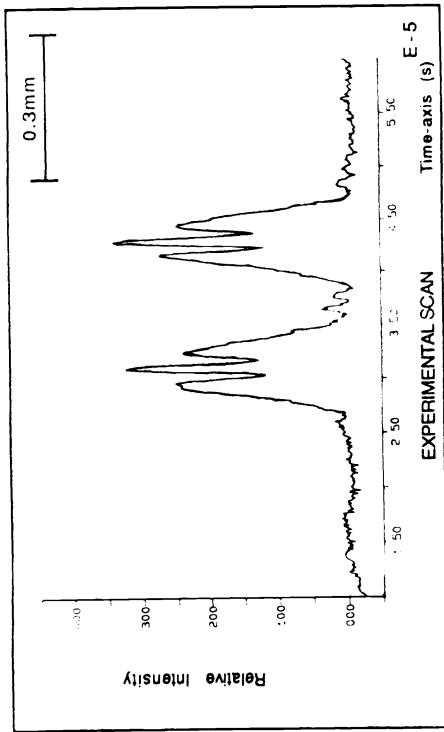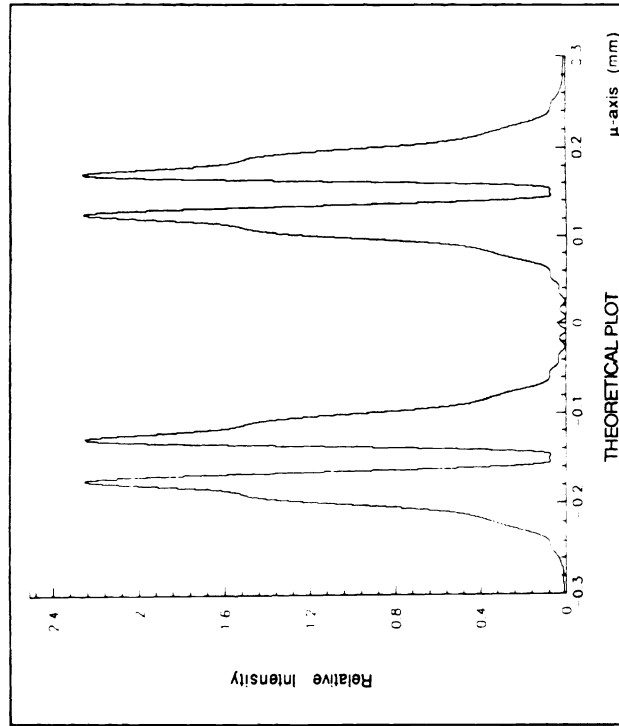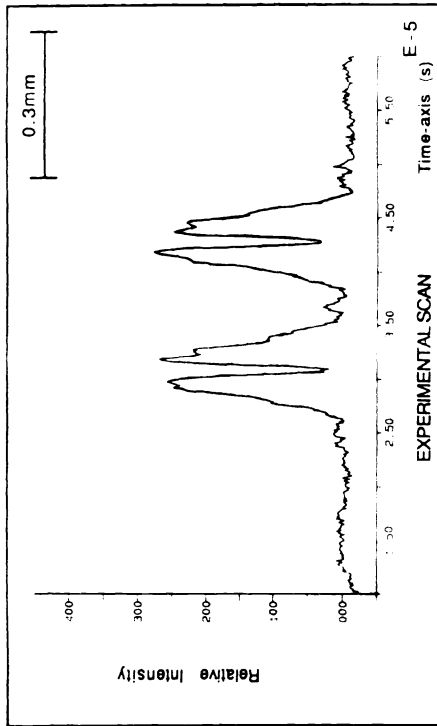
Figure 6. A comparison of experimental and numerically calculated images for $\Omega = 19.616$. The figures show the intensity along a line joining the common centres of two discs separated by $2b = 300\,\mu m$ for $\Delta Z = 0.0$, $\Delta Z = -3.00$, and $\Delta Z = -4.50$.
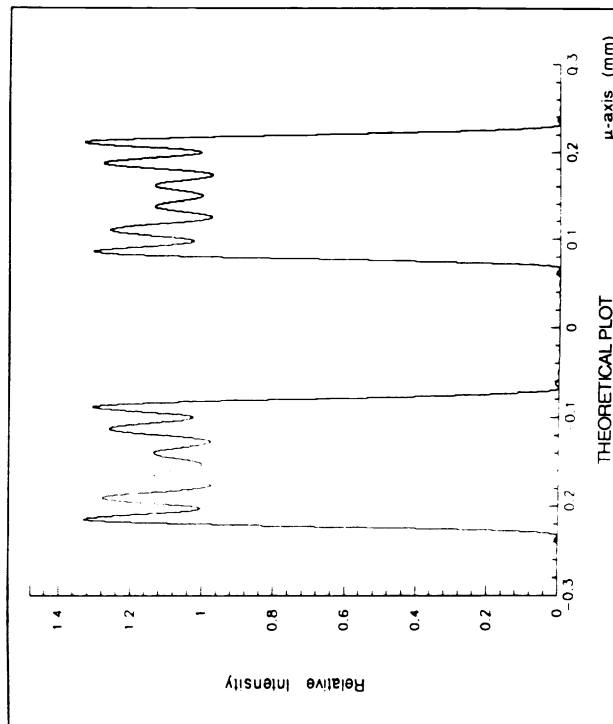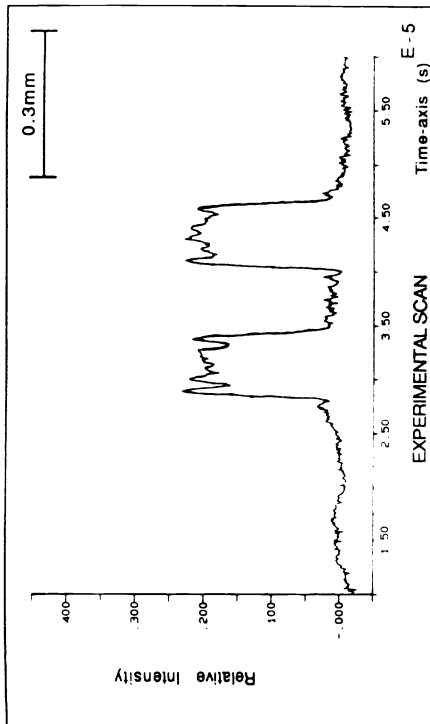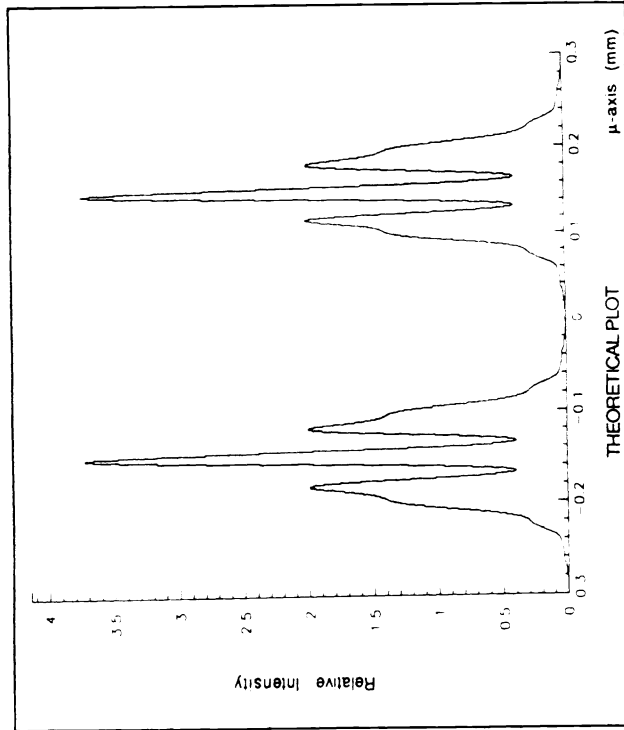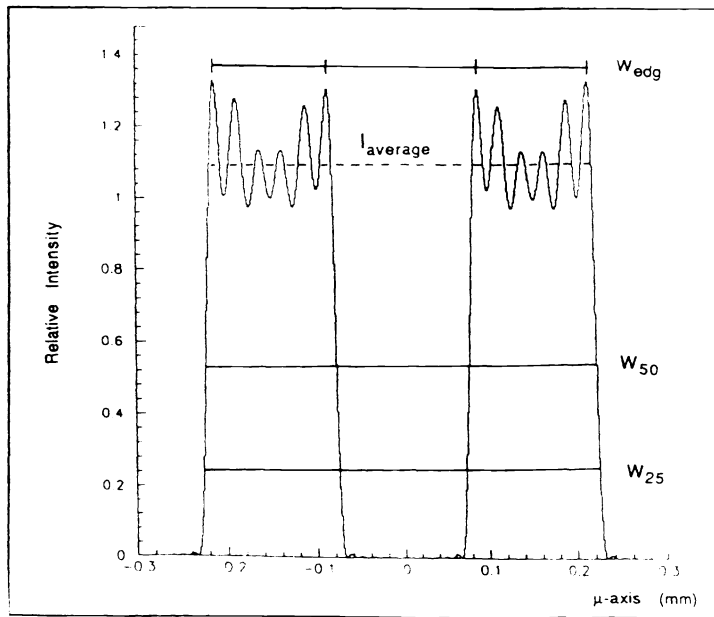
(b)

(c)

Figure 7. The measurement criteria used in this work (after Belz and Shofner [5]).

Table 1. Diameter and separation for criterion W_{25}.

Ω	7·016	10·173	13·324	19·616
Touching discs, 2 × nominal diameter: 300 µm				
Theoretical 2D	300·0 µm	302·0 µm	300·0 µm	295·0 µm
Experimental 2D	289·0 µm	301·0 µm	289·0 µm	295·0 µm
Nominal diameter: 150 µm, nominal separation 75 µm				
Theoretical D	157·0 µm	148·0 µm	150·0 µm	150·0 µm
Experimental D	170·0 µm	150·0 µm	146·0 µm	147·0 µm
Theoretical S	65·0 µm	78·0 µm	74·0 µm	74·0 µm
Experimental S	41·0 µm	66·0 µm	69·0 µm	69·0 µm
Nominal diameter: 150 µm, nominal separation 150 µm				
Theoretical D	157·0 µm	148·0 µm	150·0 µm	150·0 µm
Experimental D	160·0 µm	150·0 µm	150·0 µm	145·0 µm
Theoretical S	138·0 µm	154·0 µm	150·0 µm	150·0 µm
Experimental S	130·5 µm	139·0 µm	139·0 µm	145·0 µm

Table 2. Diameter and separation for criterion W_{50}.

Ω	7·016	10·173	13·324	19·616
Touching discs, 2 × nominal diameter: 300 μm				
Theoretical 2D	291·0 μm	291·0 μm	291·0 μm	291·0 μm
Experimental 2D	277·0 μm	289·0 μm	283·0 μm	289·0 μm
Nominal diameter: 150 μm, nominal separation 75 μm				
Theoretical D	140·0 μm	136·0 μm	143·0 μm	145·0 μm
Experimental D	151·0 μm	141·0 μm	141·0 μm	145·0 μm
Theoretical S	80·0 μm	90·0 μm	78·0 μm	78·0 μm
Experimental S	64·0 μm	72·0 μm	72·0 μm	72·0 μm
Nominal diameter: 150 μm, nominal separation 150 μm				
Theoretical D	140·0 μm	136·0 μm	141·0 μm	145·0 μm
Experimental D	145·0 μm	141·0 μm	145·0 μm	139·0 μm
Theoretical S	157·0 μm	161·0 μm	159·0 μm	152·0 μm
Experimental S	145·0 μm	150·0 μm	145·0 μm	147·0 μm

Table 3. Diameter and separation for criterion W_{edg}.

Ω	7·016	10·173	13·324	19·616
Touching discs, 2 × nominal diameter: 300 μm				
Theoretical 2D	240·0 μm	252·0 μm	261·0 μm	272·0 μm
Experimental 2D	232·0 μm	249·0 μm	257·0 μm	266·0 μm
Nominal diameter: 150 μm, nominal separation 75 μm				
Theoretical D	83·0 μm	97·0 μm	111·0 μm	125·0 μm
Experimental D	95·0 μm	110·0 μm	116·0 μm	124·0 μm
Theoretical S	143·0 μm	125·0 μm	115·0 μm	97·0 μm
Experimental S	113·0 μm	104·0 μm	104·0 μm	93·0 μm
Nominal diameter: 150 μm, nominal separation: 150 μm				
Theoretical D	83·0 μm	97·0 μm	111·0 μm	125·0 μm
Experimental D	81·0 μm	104·0 μm	116·0 μm	116·0 μm
Theoretical S	219·0 μm	208·0 μm	189·0 μm	171·0 μm
Experimental S	208·0 μm	191·0 μm	174·0 μm	147·0 μm

6. CONCLUSIONS

In this paper we have derived an expression for the three-dimensional image structure obtained from finite aperture Fraunhofer holograms of two identical co-planar objects.

We have numerically solved the resulting integrals for the simple but important case of two opaque discs.

We have developed a simple, rapid, and accurate technique for measuring the intensity in a replayed hologram image across a single video line. By averaging and background subtraction we have acheived a good signal-to-noise ratio. For our purposes this technique has advantages over the traditional photographic densitometry used by previous authors.

We have shown that an excellent qualitative agreement exists between the numerical data and the measured image intensities. We have confirmed the general features of these disc images, found in the single object case by Belz and Shofner[5]. Using their measurement criteria for both disc diameter and separation we have confirmed their conclusion that W_{50} is accurate experimentally, and have additionally shown that it is also useful for determining the disc separation. However we found no significant improvement over the criterion W_{25}, this we attribute to the very low noise levels in our holograms, and expect that for noisy images W_{50} would give the most accurate measurements.

For a given limiting aperture two congruent objects of signifficantly different sizes would be recorded with differing resolutions, and our results will not be directly applicable to this case, however we beleive that our conclusions regarding measurement criteria will still apply.

We intend to continue this work by extending the theory to encompass two identical non-coplanar objects. This will enable us to model the depth resolution of Fraunhofer holography, something that is known in practice to be very poor [3]. We will design a precision three-dimensional test object to enable us to verify the prediction of this extended model. In addition we intend to test our hypothesis that a combination of maximizing the edge sharpness and minimizing the intensity variation across the disc diameter image processing techniques on both simulated and experimental images.

Acknowledgements

7. REFERENCES

1. Thompson B.J., *J.Phys.E: Sci. Instrum.* **7**, 781-8, 1974

2. Grabowski W., *Opt.Laser Technol.* **15**, 199-205, 1983

3. Hobson P.R., Imrie D.C., Lush G.J., *Nucl.Instrum. Methods* **A239**, 155-9, 1985

4. Thompson B.J., Malyak P.H., *Proc. SPIE* **573**, 12-20, 1985

5. Belz R.A., Shofner F.M., *Appl.Optics* **11**, 2215-22, 1972

6. Raouf A., *Three dimensional image structure in in-line Fraunhofer holography*, Ph.D. Thesis, Brunel University, 1991

7. Tyler G.A., Thompson B.J., *Optica Acta* **23**, 685-700, 1976

8. Belz R.A., *An investigation of the real image reconstructed by an in-line Fraunhofer Hologram aperture-limited by film effects*, Ph.D. Thesis, University of Tennessee, 1971

9. Engels H., *Numerical Quadrature and Cubature*, Academic Press, London, 1980

10. Abramowitz M., Stegun I.A., *Handbook of Mathematical Functions*, p919, Dover, New York, 1972

11. LAZA Holograms, 47 Alpine Street, Reading, RG1 2PY, UK